Fatigue & Fracture of Engineering Materials & Structures

WILEY

FFEMS Fatigue & Fracture of Engineering Materials & Structures

SPECIAL ISSUE ARTICLE OPEN ACCESS

A Novel Approach for ΔK Estimation in the Fatigue Threshold Region Based on ΔK_{th} and $K_{max,th}$

Pablo M. Cerezo | Jose A. Aguilera | Alejandro S. Cruces | Pablo Lopez-Crespo

Department of Civil and Materials Engineering, University of Malaga, Malaga, Spain

Correspondence: Pablo Lopez-Crespo (plopezcrespo@uma.es)

Received: 19 December 2024 | **Revised:** 28 October 2025 | **Accepted:** 1 November 2025

Funding: Authors would like to acknowledge the following financial support: "FEDER Programa Operativo" by "Junta de Andalucía" (Spain)—grant reference UMA18-FEDERJA-250. Funding for open access charge: Universidad de Malaga/CBUA. This research was also supported by an FPU grant (Formación de Profesorado Universitario) from the Spanish Ministry of Science and Innovation (MCINN) to P.M.C. through grant number FPU23-03834. The authors would also like to acknowledge helpful discussions with Prof. D. Kujawski.

Keywords: fatigue crack growth (FCG) | near-threshold | plasticity-induced crack closure (PICC) | stress intensity factor (SIF)

ABSTRACT

A novel procedure, proposed by Kujawski and Vasudevan [1], has been evaluated as an alternative to the ASTM E647 standard for determining the ΔK_{th} and $K_{max,th}$ thresholds. This method relies solely on the actual propagation of cracks, which occurs only when both thresholds are satisfied simultaneously. For long cracks, a more efficient estimation of thresholds can be achieved. Compared to the ASTM E647 standard ($R = 0.1$, $\Delta K_{th} = 2.95\,MPa\sqrt{m}$), the new methodology for the same R yielded a value of $\Delta K_{th} = 2.50\,MPa\sqrt{m}$ and determined a maximum stress threshold of $K_{max,th} = 3.35\,MPa\sqrt{m}$. A correlated parameter, $K^* = K_{max}{}^{\alpha} \cdot \Delta K^{1-\alpha}$, $\alpha = 0.5$ for Al 2024 T3 alloy, was employed to provide an effective relation between the loading ratio and the threshold conditions, with K* values ranging from 2.8 to $3\,MPa\sqrt{m}$ for R-ratios from 0.1 to 0.7. The implementation of this technique has the potential to reduce testing time and postprocessing efforts by minimizing the need for crack propagation calculations. This method provides valuable insights into the material behavior near the fatigue threshold for the specific cases and material investigated.

1 | Introduction

An in-depth understanding of fatigue crack growth (FCG) rate is critical for the reliable prediction of the safe operational life of components in service. Moreover, the near-threshold regime is key for the proper establishment of inspection intervals, which in turn safeguards the integrity and longevity of such structural elements. FCG occurs in the near-threshold region for an average crack growth rate below 10^{-9} m/cycle [1]. In this region, the stress intensity factor (SIF) reaches the SIF range at threshold (ΔK_{th}), which indicates a material's resistance to the propagation of cracks. ΔK_{th} represents the SIF range (ΔK) value below which FCG does not occur [2]. ΔK_{th} is also a limit for damage tolerance design (DTD) [3, 4], where a mere 1-$MPa\sqrt{m}$ change could lead to an approximately 18% variation in residual life [5–7]. Determining ΔK_{th} involves a complex and intricate process that is not easily straightforward. This is due to the qualitative and quantitative variations arising from the use of different experimental, numerical, and analytical methods, along with their corresponding assumptions [6]. FCG curves, associated with physically small crack and those associated with microstructurally small crack, demonstrate distinct morphological characteristics [8]. Some studies have demonstrated [9] that crack propagation may continue even when the measured long-crack threshold, as defined by the ASTM test procedure [1, 3], has been surpassed. Hence, ΔK_{th} is defined as the critical value of ΔK at which the crack growth rate (da/dN) falls below 10^{-10} m/cycle [3, 10].

Summary

- This work applies the Kujawski and Vasudevan method as an alternative to the ASTM standard.
- The method reduces testing time and facilitates adaptive load adjustments.
- The K* parameter is employed to assess the R-ratio's impact on fatigue crack growth in Al 2024-T351.
- Combining ΔK_{th} and $K_{max,th}$ provides a reliable evaluation of fatigue thresholds.

Numerous research studies have examined the near-threshold fatigue of engineering alloys [11, 12]. The variation of threshold values associated with different microstructures within the same alloy is significantly reduced at elevated R values in comparison to lower R values [13]. Instead of contributing to the R values, the contribution of $K_{max,0}$ has been introduced, where $K_{max,0} = \Delta K_0/(1\text{-}R)$, [14]. The threshold conditions for crack growth rate are overseen by two important driving force parameters, ΔK_0 and $K_{max,0}$. A constant value of $K_{max,0}$ establishes the threshold at low R values. Meanwhile, a constant value of ΔK_0 determines the threshold conditions at high R values [15, 16].

The method for obtaining ΔK_{th} is standardized by ASTM 647 [1] or ISO 12108 [17] and involves a gradual reduction of the load for a constant R in a specimen after the precracking stage. This load-shedding process has undergone considerable criticism through the years [18, 19]. When the field ΔK is abruptly reduced, the growth of the current crack at the tip, the largest previous plastic zone, which developed at the previous higher load level, can result a complete stop or in a retardation of FCG. In contrast, if the ΔK values are decreased gradually, certain materials may exhibit crack closure, resulting in early contact of the crack faces. This phenomenon can yield a seemingly elevated ΔK_{th} value due to oxidation on the fracture surfaces and crack tip. The selection of a specific ΔK value can be somewhat arbitrary, significant experimental uncertainties and errors can impact the assessment of fatigue thresholds. Additionally, as the enforced ΔK diminishes with growing crack length, the crack growth detention threshold is measured rather than the initiation crack growth threshold. The latter aspect is more important in most practical situations [20].

Several methodologies have been proposed to address these limitations. A new technique was proposed based on entirely compressive cyclic loads to induce self-arresting fatigue precracks in notched specimens, aiming to enhance their structural integrity and fatigue life [18, 19]. The material is exposed to cyclical tensile loads that start below ΔK_{th}. If no crack growth is observed, the ΔK value is gradually increased until the threshold for crack growth is reached. Once the desired intensity is reached, a constant cyclic load level of the fatigue test can be conducted.

A method of increasing the load ratio (R) for measuring an intrinsic fatigue threshold was popularized [21]. Maximum SIF (K_{max}) is maintained at a constant level, while ΔK is gradually reduced by increasing *R*. When K_{max} remains constant, the dimensions of the plastic zone at the crack tip remain invariant. Consequently, a reduction in load is not anticipated to induce the typical retardation effects associated with variable amplitude fatigue. Furthermore, at the high load ratio levels where ΔK_{th} is measured, crack face closure is nearly eliminated, making this method not suitable for investigating how load ratio affects crack growth rates near the threshold [22, 23].

It is important to recognize that the use of various methods to determine fatigue thresholds has led to notable variations in data accuracy and interpretation [20]. Care must be taken when analyzing crack growth mechanisms, as testing artifacts can easily overshadow the intrinsic effects of microstructural or mechanical factors. Additionally, the operational definition of ΔK_{th} is slightly subjective and varies across different techniques.

The threshold regime is influenced by microstructural features, for example, grain size and slip characteristics across various alloy systems. This phenomenon has been documented in aluminum alloys [24–26], ferrous alloys [27, 28], titanium alloys [29, 30], and nickel-base superalloys [31]. This accumulation of knowledge underscores the complexity and significance of microstructural influences on fracture mechanics within these material classes.

Aluminum alloy 2024-T351, a widely used aerospace material, is particularly susceptible to fatigue damage due to its inherent microstructure and the aggressive environments in which aircraft operate [32]. The high strength-to-weight ratio and excellent corrosion resistance of 2024-T351 make it a preferred choice for various aircraft components, including wings, fuselage, and landing gear. However, the cyclic stresses encountered during flight operations can lead to the initiation and propagation of fatigue cracks, ultimately compromising the structural integrity of these critical components [33, 34].

The transition between the Paris regime and the near-threshold regime generally occurs when the radius of the cyclic plastic zone (r_c) approaches the characteristic microstructural dimension of the alloy, grain-size diameter (d_g) in this case. This transition is realized when the Δ attains the SIF range at the knee transition point (ΔK_n). Beyond this threshold, the growth behavior exhibits insensitivity to microstructural variations [30].

Roughness of the surface near a crack and the size of the grains near the crack tip also impact Δ_{th} [3, 35]. Larger grain sizes promote simultaneous oxide-induced crack closure (OICC) and roughness-induced crack closure (RICC) [36], resulting in higher Δ_{th} values when measured [37]. Therefore, in the load reduction method, rough surfaces can produce rubble that leads to early crack closure and increased Δ_{th}. The Δ_{th} diverges from mechanically long and short cracks. Only in small-scale yielding conditions in long cracks, linear-elastic fracture mechanics (LEFM) can be applied. In the literature [38], two distinct Δ_{th} levels can be found: a microstructural threshold applicable to short crack and a mechanical threshold relevant for long cracks [39].

In order to consistently generate R-ratio data, ASTM E647 [1] recommends a load reduction test procedure in the near-threshold and threshold regions. Researchers have found that this procedure may lead to higher thresholds, ΔK_{th}, which are attributed to remote plasticity-induced crack closure (PICC) resulting from the load reduction process [22, 23] and the induced load-history

effects on crack growth rate. This leads them to suggest that the ASTM standard may have an error in measuring ΔK_{th}. In experiments conducted at the near-threshold range, challenges have arisen due to the low resolution in measuring crack opening SIF (K_{OP}). Many authors [22, 23] have noted the difficulty in making these measurements at this level, which allows for computing the threshold value but is insufficient for consistent correlation with the near-threshold FCG behavior [23, 37].

A detailed description of FCG requires consideration of two SIF parameters: ΔK and K_{max} [40, 41]. The proposal suggests that for a crack to propagate, both ΔK_{th} and $K_{max,th}$ thresholds must be simultaneously satisfied. If only one threshold is met, the crack will not propagate. Therefore, for a crack extension to occur, the applied ΔK must exceed ΔK_{th}, and the applied K_{max} must surpass $K_{max,th}$. While there is an ASTM Standard (E-647) for measuring ΔK_{th}, no standard procedure was proposed for $K_{max,th}$ [42].

This article introduces the approach proposed by Kujawski [42] to characterize the ΔK_{th} and threshold at maximum SIF ($K_{max,th}$) of aluminum alloy 2024-T351 samples. For the first time, this methodology effectively overcomes the limitations and drawbacks associated with existing standards. The implementation of this innovative technique aims to enhance the accuracy and reliability of the assessment of material properties, thereby improving its applicability in the fields of engineering and structural design.

2 | Material, Samples, and Setup

Compact tension (CT) specimens were employed under mode I loading conditions with constant cyclic loads. The materials utilized in this study were sourced from an aluminum 2024-T351 plate, the composition of which is presented in Table 1. The samples were cut in the T-L direction, facilitating crack propagation in alignment with the rolling direction. The dimensions of the samples are shown in Figure 1a, while the sample itself is presented in Figure 1b. The experimental setup was similar to that described previously [44]. Three specimens were used for the various R-ratios. Table 2 presents the mechanical properties of the aluminum alloy 2024-T351.

Prior to conducting any tests, the CT specimens undergo a sand polishing process (1200 grade SiC sandpaper) to enhance the accuracy of determining crack positions. In preparation for the fatigue test, these specimens are precracked to eliminate the nucleation phase, thereby allowing for a focused examination of crack propagation.

The fatigue crack initiation and propagation tests were conducted using the Walter + Bai LFM-C 5 kN in situ fatigue test machine. Additionally, a camera was installed to monitor crack propagation and facilitate digital measurement of crack length, serving as an additional source of data. The MATLAB Image Viewer is

TABLE 1 | Composition in weight percentage of aluminum alloy 2024-T351. The balance is Al [43].

Cu	Mg	Mn	Fe	Si	Zn	Ti	Cr
4.90–3.80	1.80–1.20	0.90–0.30	0.50	0.50	0.25	0.15	0.10

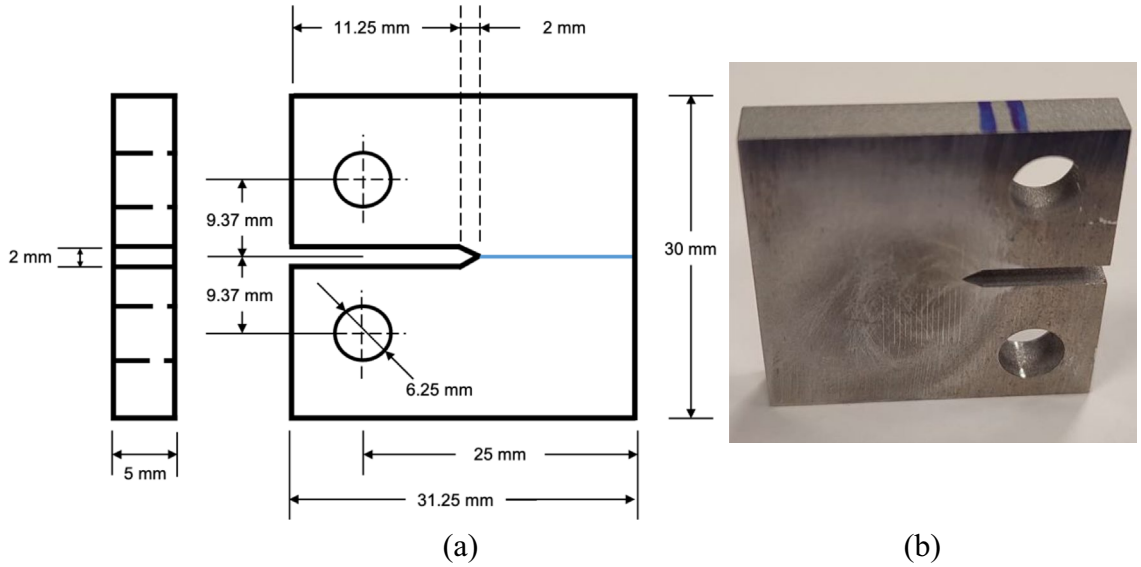

FIGURE 1 | (a) Geometry of the CT specimen, the thickness is 5 mm and the W = 25 mm according to ASTM E399 [45] and (b) image of the aluminum sample after surface preparation. [Colour figure can be viewed at wileyonlinelibrary.com]

TABLE 2 | Mechanical properties of aluminum alloy 2024-T351 [44].

Young modulus	Yield stress	UTS	Elongation at break	Brinell Hardness
73 GPa	325 MPa	470 MPa	20%	137

TABLE 3 | Initial parameters for precracking stage.

R	0.1	0.3	0.7
Sample	I	III	II
ΔK (MPa√m)	7.00	6.00	4.00
a_f (mm)	7.83	7.64	7.28
Cycles	50,000	60,000	100,000

used to measure the pixel length of the crack tip, allowing for the determination of the crack length. The precracking was conducted under mode I loading at a frequency of 10 Hz, ed Table 3 accounts for some more information about the precracking step.

The crack growth rate, denoted as da/dN, was calculated using numerical derivation in accordance with ASTM E647 [1]. This methodology entails the application of a fifth-order polynomial fitting to a series of successive points on the a-N curve. Subsequently, the growth rate is determined by calculating the derivative of the fitted polynomial. Data points on the a-N curve were selected at 2000-cycles intervals.

3 | Estimation of ΔK_{th} Through ASTM E647

ΔK_{th} values are typically measured using a technique known as load shedding. In this methodology, crack propagation begins ahead of a starter notch in a CT specimen at a ΔK value that falls within the Paris regime of crack propagation. This approach allows for the systematic evaluation of crack growth behavior under specified loading conditions. The far-field stress range, along with the corresponding ΔK value, is systematically reduced in a series of stages, no more than 10%. In each stage of the constant far-field load range, the propagation of the fatigue crack occurs over at least four times greater than the maximum extent of the current plastic zone in order to avoid the previous plastic zone's influence over the next step. This process is repeated until ΔK_{th} is reached, which is defined by either no crack growth or crack growth that is below 10^{-10} m/cycle.

The load-shedding process can induce crack closure when the crack faces come into contact before the minimum load in a fatigue cycle is reached, effectively reducing the actual driving force for crack propagation. This phenomenon can result from PICC [46] (due to residual plastic deformation at the crack tip), OICC [47], or RICC [20]. ASTM E647 acknowledges these effects and recommends maintaining a constant R to control crack closure influence. However, in low ΔK conditions, crack closure can lead to an overestimation of ΔK_{th}, as the stress effective fatigue threshold range (ΔK_{eff}), the portion of ΔK actually driving crack growth, is lower than the nominally applied ΔK.

The fatigue test was performed using a constant force-decreasing loading approach, Figure 2a. The test commenced after the precrack (in the beginning of the Paris regimen [48]), with a maximum 10% reduction in ΔK at the initial stages, Figure 2b and Table 4.

The FCG rate as a function of the ΔK for R of 0.1, 0.3, and 0.7 is presented in Figure 3, following the standard procedures. To establish the fatigue threshold, a logarithmic regression was applied

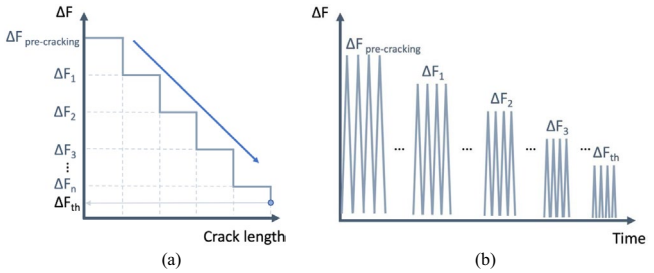

FIGURE 2 | (a) Load decreasing strategy (in each level the crack grows 0.25 mm). ΔK_{th} is reached when ΔF_{th} is met; the crack length does not change at this level. (b) Diagram of the cycles performed; for each ΔF package, the ratio R remains constant at 0.1. [Colour figure can be viewed at wileyonlinelibrary.com]

TABLE 4 | Load decreasing steps and cycles for each R-ratio until reaching near-threshold regime.

R = 0.1/ΔK (MPa√m)	R = 0.3/ΔK (MPa√m)	R = 0.7/ΔK (MPa√m)
6.30	6.00	3.70
5.67	5.40	3.44
5.10	4.87	3.33
4.85	4.38	3.16
4.61	3.87	2.92
4.38	3.45	2.59
4.16	3.11	2.31
3.95	2.79	2.27
3.75	—	2.17
—	—	2.05
—	—	1.94
—	—	1.85
—	—	1.76
—	—	1.61
572,000 cycles	845,000 cycles	1,862,000 cycles

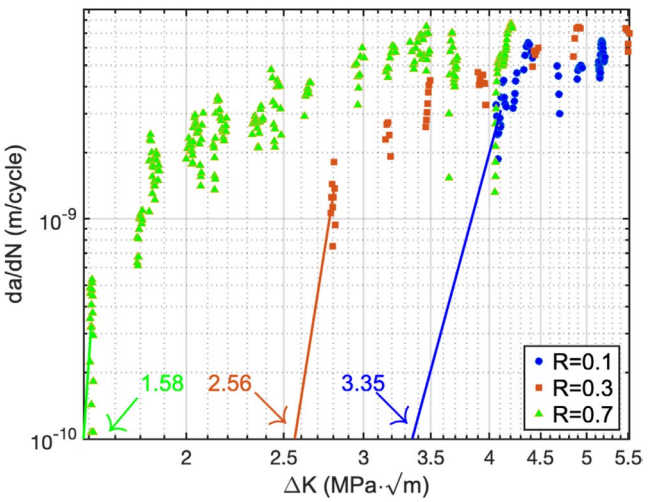

FIGURE 3 | da/dN vs. ΔK diagram of the aluminum alloy 2024-T351 following ASTM E647, showing the ΔK_{th} for R = 0.1, 0.3, and 0.7. [Colour figure can be viewed at wileyonlinelibrary.com]

where the threshold was defined at a crack growth rate of 10^{-10} m/cycle. The resulting threshold values are $\Delta K_{th} = 3.35\,MPa\sqrt{m}$ for $R = 0.1$, $2.56\,MPa\sqrt{m}$ for $R = 0.3$, and $1.58\,MPa\sqrt{m}$ for $R = 0.7$. The observed reduction in fatigue threshold with increasing R is primarily attributed to the phenomenon of PICC [37]. At low R values, the crack experiences greater closure due to residual plastic deformation in the wake of the crack tip, effectively diminishing the ΔK_{eff} driving crack propagation [49, 50]. This explains the highest threshold observed at $R = 0.1$, as a greater portion of the applied ΔK is counteracted by crack closure effects.

As the R increases, the crack remains more open throughout the loading cycle, diminishing the influence of plastic-induced crack closure and leading to a lower fatigue threshold. This trend is evident when comparing the threshold values for $R = 0.3$ and $R = 0.1$, where the reduction in threshold at the higher R-ratio is attributed to a diminished crack closure effect. This effect becomes even more pronounced at $R = 0.7$, as the higher minimum load ensures the crack remains open for a greater portion of the loading cycle, minimizing the impact of crack closure and resulting in the lowest threshold value.

4 | Procedure for Determining ΔK_{th} by Kujawski

A method for determining the threshold that considers the influence of crack tip closure has been proposed by Kujawski [42], which was partially derived from early works [22, 37]. This method establishes the dependence of the crack growth threshold on two parameters: ΔK_{th} and $K_{max,th}$, for a specific *R*. The proposed approach eliminates the lengthy load reduction procedure outlined in ASTM standards, which fails to adequately account for the effects of precracking load history on ΔK_{th}. Furthermore, the ASTM standard lacks clear guidance on how to determine the $K_{max,th}$.

The procedure is illustrated in Figure 4, which comprises two steps. First, $K_{max,th}$ is determined, as shown in Figure 4a. Then ΔK_{th} is obtained through the process depicted in Figure 4b. Initially, a set of load cycles ($N^* = 10$) is applied at the K_n for the specified *R*, followed by a small increment in ΔK for 10^5 cycles. This process is repeated in steps, progressively increasing ΔK until crack propagation is observed. The ΔK value at which crack propagation begins defines ΔK_{th}.

The $K_{max,th}$ procedure depicted in Figure 4a involves pausing the crack growth test at the minimum SIF (K_{min}), while the ΔK_{th} procedure in Figure 4b reaches a maximum K determined by

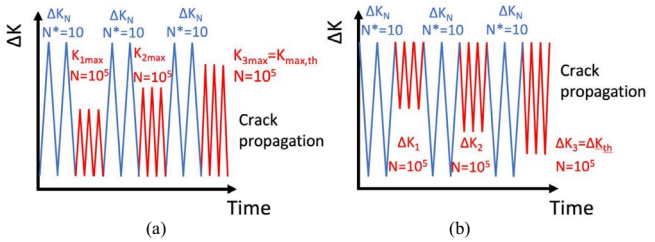

FIGURE 4 | Schematic representation of loading procedures for measuring (a) $K_{max,th}$ with increasing K_{max} at constant K_{min} and (b) ΔK_{th} with decreasing K_{min} at constant K_{max}. [Colour figure can be viewed at wileyonlinelibrary.com]

K_{max}. Both procedures initiate every step with an initial set of 10 load cycles ($N^* = 10$) applied at a specified *R*. This serves three critical purposes: (1) stabilizing the material after each block of loading, (2) creating striations on the fracture surface for further validation of test results, and (3) minimizing the residual stress resulting from precracking. Following this, a small increment (5% to 10%) in K_{max} is introduced, and the loading is maintained for 10^5 cycles. The process is systematically conducted through successive steps, with progressively increasing K_{max} values until the initiation of crack propagation is observed; in the previous steps, no propagation occurs. The K_{max} value at which crack propagation commences establishes the $K_{max,th}$ value.

For the experimental investigations, various R-ratios of 0.1, 0.3, 0.5, 0.7, and 0.9 were employed. The ΔK_n values were determined in accordance with the ASTM testing standards, aligning with prevailing literature [50–52].

The $R = 0.1$ test is described in detail. Following an initial 10 cycles at ΔK_n, an additional 10^5 cycles were performed at a K_{1max} of $2.79\,MPa\sqrt{m}$ (this value was chosen because it is smaller than K_{max} of ΔK_n), with no observed crack propagation. Subsequently, two further stages were performed, leading to a final stage where crack growth was detected. Consequently, the $K_{max,th}$ was determined to be $3.35\,MPa\sqrt{m}$, Figure 5a.

After determining the $K_{max,th}$ value, the researchers subjected a new portion of the same specimen to testing by performing 10 cycles of ΔK_n, followed by applying a ΔK of $2.50\,MPa\sqrt{m}$ for 10^5 cycles, during which crack propagation was observed. This indicated that the limit had been reached. Regardless of whether ΔK is increased or decreased between loading steps, the method remains valid because, after each increment or decrement, the material at the crack tip is reconditioned through the application of an overload cycle at a higher ΔK_n. This procedure effectively resets the crack tip conditions, allowing crack propagation to restart from a comparable mechanical state. As a result, the sequence of ΔK variations (increasing or decreasing) does not influence the identification of the threshold. If, during a decreasing ΔK sequence, crack propagation ceases at a given ΔK value while it was observed at the previous higher ΔK value, the threshold can be determined between these two points. Similarly, if, during an increasing ΔK sequence, crack propagation is not initially observed but initiates at a higher ΔK value, the threshold corresponds to the last ΔK value at which propagation was observed. To confirm that this was indeed the threshold, an additional test was conducted to assess crack propagation below this level. The results indicated no crack propagation, thus confirming that the previously established threshold value of ΔK at $2.50\,MPa\sqrt{m}$ is valid, as illustrated in Figure 5b, to which 500,000 cycles have been applied.

One might think that this threshold value differs from the value obtained through the ASTM standard, as the threshold was initially measured at $\Delta K_{th} = 3.35\,MPa\sqrt{m}$. However, this is primarily due to its significant dependence on the R-ratio. In this scenario, with a K_{max} of $4.42\,MPa\sqrt{m}$, the K_{min} is $1.92\,MPa\sqrt{m}$ when ΔK_{th} is $2.50\,MPa\sqrt{m}$ and R is 0.43; for R equal to 0.1, ΔK_{th} is $3.35\,MPa\sqrt{m}$, Figure 6a. Literature suggests that low R ratio values can result in plasticity effects, which affect crack closure under plain stress conditions, with the K_{OP} not being null

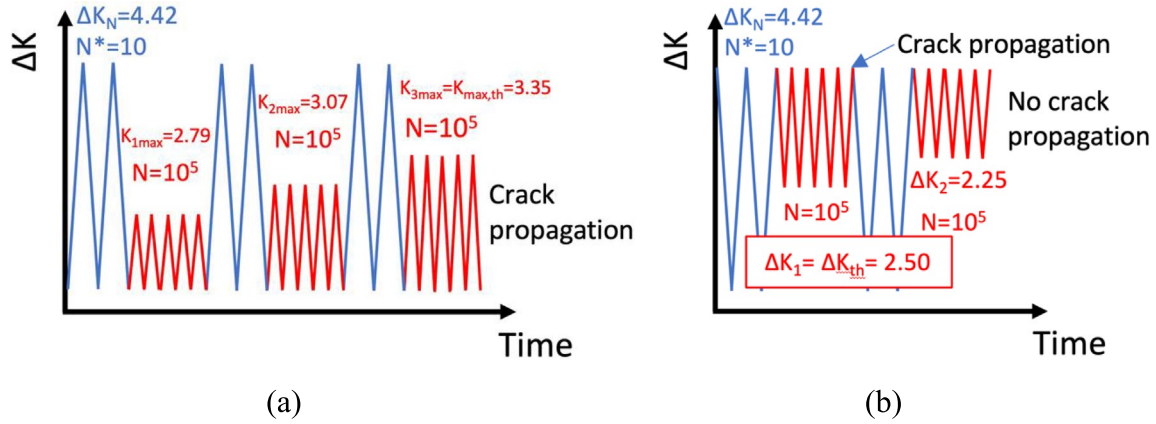

FIGURE 5 | Historical sequence of SIF used to determine (a) $K_{max,th}$ and (b) ΔK_{th} for R = 0.1. The units for ΔK and K are MPa$\sqrt{m}$. [Colour figure can be viewed at wileyonlinelibrary.com]

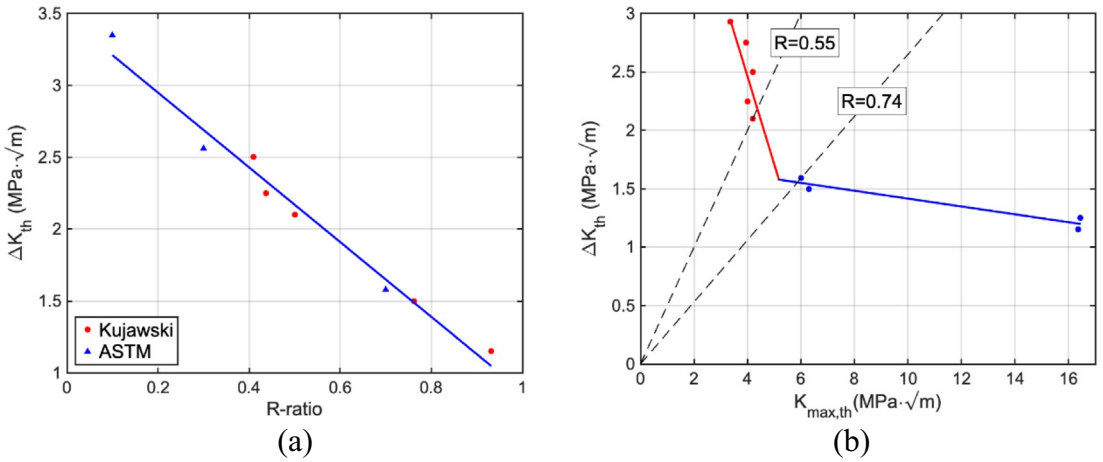

FIGURE 6 | (a) ΔK versus R-ratio for ASTM and Kujawski data and (b) ΔK_{th} as a function of $K_{max,th}$ along with data collected for a growth rate of 10^{-10} (m/cycle). [Colour figure can be viewed at wileyonlinelibrary.com]

[15, 53, 54]. The main parameters for the remaining R-ratios are quantitatively presented in Table 5 and Figure 6b.

The influence of the R on near-threshold fatigue crack propagation is frequently attributed to crack closure, which is commonly associated with the RICC mechanism. In the present investigation, the closure phenomenon was estimated using a linear equation within the near-threshold regime. Within this regime, the R is consistently affected by the crack closure effects, Figure 6a. As the ΔK_{th} decreases with increasing *R*, this suggests that even at high R values, the K_{op} remains higher than the K_{min}.

The most demonstrating representation of the transition from a "closure-affected" to a "closure-free" threshold is depicted in a plot of ΔK_{th} versus $K_{max,th}$ in Figure 6b. The distinct change in slope observed strongly suggests a shift in the governing mechanism, concurrent with the elimination of global crack closure. Assuming a closure-affected behavior, both the closure SIF (K_{cl}) and the effective threshold SIF range ($\Delta K_{eff,th}$) are unaffected by *R*, there exists a critical load ratio (R_c) at which $K_{min} = K_{cl}$, as shown in Equation (1).

$$\Delta K_{eff,th} = \begin{cases} K_{max,th} - K_{cl} < \Delta K_{th}, & if\ R < R_c\ \left(K_{min,th} < K_{cl}\right) \\ K_{max,th} - K_{min,th} = \Delta K_{th}, & if\ R > R_c\ \left(K_{min,th} > K_{cl}\right) \end{cases} \quad (1)$$

TABLE 5 | Key parameters derived from the threshold calculation using Kujawski procedure.

R	0.1	0.3	0.5	0.7	0.9
ΔK_n	3.79	2.80	2.10	1.89	1.69
ΔK_{th} (MPa$\sqrt{m}$)	2.50	2.25	2.10	1.50	1.15
$K_{max,th}$ (MPa$\sqrt{m}$)	3.35	3.95	3.80	6.00	16.45
K* (MPa$\sqrt{m}$)	2.89	2.98	2.82	3.00	4.35

Under these conditions, $K_{max,th}$ is independent of the *R* below the critical value R_c. Conversely, the ΔK_{th} is independent of *R* above R_c. When plotted as $K_{max,th}$ versus ΔK_{th}, this transition manifests as a distinct "L" shape, indicating that the value of ΔK_{th} is independent of K_{max} when $R > R_c$, where global closure is no longer effective. The Schmidt and Paris [15] analysis reveals this transition approximation, where at *Rs* similar to R_c at which point K_{min} equals K_{cl}.

As observed in Figure 6a and previously [55], this behavior is not universal. In most cases, the value of ΔK_{th} is not invariant at $R > R_c$, but rather decreases with increasing *R*. This suggests that either the Schmidt and Paris model is not properly described at

$R > R_c$, or that additional mechanisms are at play. The R_c for this material is observed to be in the interval 0.55–0.74 and cannot be observed in Figure 6b.

ΔK_{th} can also be theoretically determined for ductile materials, given that the propagation of fatigue cracks is largely governed by local cyclic plasticity occurring at the crack tip [56]. By using the Burgers vector (b) and the elastic modulus of the aluminum alloy (E), $\Delta K_{th,threoretic}$ is calculated through the Hertzberg's observation [57], Equation (2). For the 2024-T351 aluminum alloy, E = 73 GPa, Table 2, and $b = a/\sqrt{2}$, where a = 0.405 nm [57]. Therefore, the value of the $\Delta K_{th,threoretic}$ for the 2024-T351 Al is 1.24 MPa$\sqrt{m}$, which is consistent with Figures 3 and 6, where ΔK_{th} for R = 0.7 is 1.58 MPa$\sqrt{m}$.

$$\Delta K_{th,\ theoretic} \propto E \cdot \sqrt{b} \tag{2}$$

Kujawski introduces a driving force parameter for crack growth that overlays the da/dN versus ΔK curves for different R-ratios. This framework enables a strong correlation between the effects of the R-ratio and the rates of crack propagation, along with the corresponding threshold conditions, Equation (3) [14, 51].

$$K^* = \left(K_{max}\right)^{\alpha} \cdot \left(\Delta K^{+}\right)^{1-\alpha} \tag{3}$$

α is a parameter assumed to be dependant of the material, and for the aluminum alloy 2024-T351 is observed to be 0.5 [14, 51], and ΔK^+ is the positive part of the range of the applied SIF. By calculating the two relevant parameters and employing K* as the fatigue crack driving force, the distant crack growth curves converge into a single curve, as illustrated in Figure 7. The influence of crack closure for varying R-ratios is disregarded, resulting in the coincidence of the curves.

The K* values corresponding to the threshold levels across the R-ratio range of 0.1–0.7, as shown in Table 5, fall within the range of 2.8–3 MPa$\sqrt{m}$. These results are consistent with previous research [14, 51], suggesting that the K* parameter is properly calibrated to align with the values specified by the ASTM standard after collapse, Figure 7.

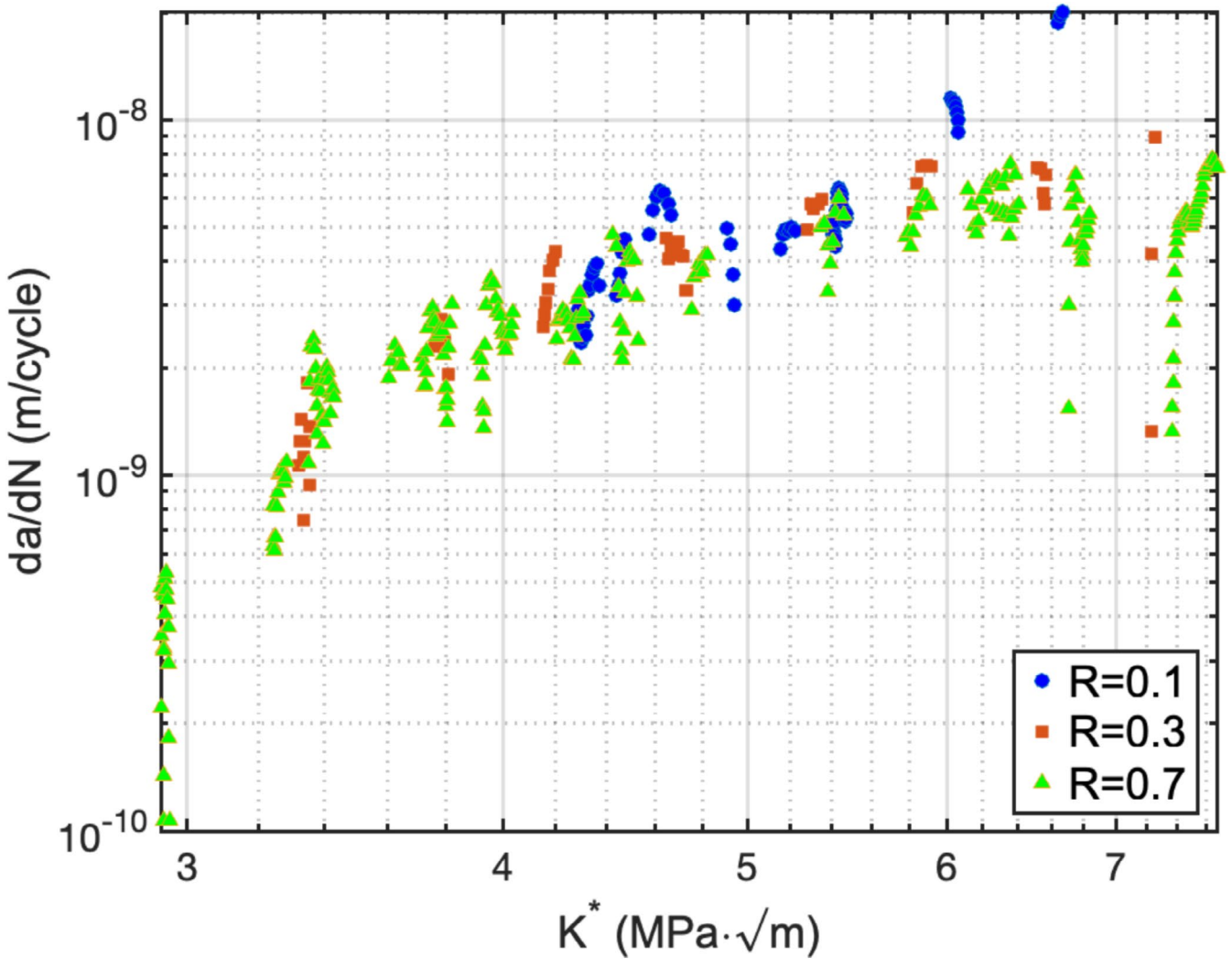

FIGURE 7 | Fatigue crack growth data of 2024-T351 Al for $K^* = \left(K_{max}\right)^{\alpha} \cdot \left(\Delta K^{+}\right)^{1-\alpha}$ and R = 0.1, 0.3 and 0.7, when $\alpha = 0.5$. [Colour figure can be viewed at wileyonlinelibrary.com]

5 | Discussion

The traditional methodology for fatigue threshold determination, mainly represented by the ASTM E647 standard [1], Figure 2, suffers from several significant limitations that may compromise the accuracy and practical applicability of the results. As pointed out in the article, the ASTM load reduction procedure can induce premature crack closure due to PICC generated in previous loading stages [22, 23]. This situation leads to an overestimation of the ΔK_{th} value, since the actual ΔK_{eff} is lower than the nominally applied ΔK [58]. Figure 3 illustrates the transition from $R = 0.1$ to $R = 0.7$, where ΔK_{th} decreases from 2.95 to 1.47 $MPa\sqrt{m}$ due to PICC influence in the ASTM standard, as the theoretical threshold is set to be 1.24 $MPa\sqrt{m}$, where there is no influence of any crack closure. Furthermore, the ASTM standard focuses primarily on the determination of ΔK_{th} without providing standardized guidance for obtaining $K_{max,th}$, a parameter that, according to many authors [40, 41, 59], is equally critical for defining the threshold conditions for fatigue crack propagation.

In contrast to the ASTM approach, the methodology proposed by Kujawski [42] represents a significant innovation in addressing these fundamental deficiencies. His procedure, schematized in Figure 4, is based on an independent and sequential determination of $K_{max,th}$ and ΔK_{th} by stepwise increments in the relevant loading parameters and direct observation of crack propagation initiation. This approach mitigates the influence of the load history associated with the gradual load reduction of the ASTM method, thus minimizing the effects of remote PICC that can distort the threshold measurement. The inclusion of the concept of $K_{max,th}$ as an independent threshold parameter recognizes the importance of the maximum stress level at the crack tip for fatigue propagation, especially in near-threshold regimes. Although the estimated cycle counts range from 500,000 to 572,000–1,862,000 for the new procedure in comparison to ASTM standards, the time spent on postprocessing is significantly reduced, as the crack position does not need to be calculated at each step, as is required for ASTM standards.

In Figures 3 and 6a, the various thresholds derived from the ASTM method illustrate the significant impact of PICC, recognized as the principal contributor to the crack closure effect [37]. This influence leads to a decrease in the threshold value from 2.95 to 1.47 $MPa\sqrt{m}$ for $R = 0.7$ and 0.1.

The parameter K* is introduced to serve as a threshold indicator, coinciding with the ΔK_{th} for R close to 0. This relationship can be associated with any experimental value corresponding to $K_{max,th}$ or ΔK_{th} for a specified R, Equation (3). As depicted in Table 5 and Figure 7, the K* value offers pertinent information that can be extrapolated to the remaining R-ratio conditions. The article reveals that the K* value typically ranges from 2.8 to 3 $MPa\sqrt{m}$, except for the $R = 0.9$ case, where it rises to 4.35 $MPa\sqrt{m}$, possibly due to the limited extension of the α parameter that influences Equation (3), where K* is calculated, to high R-ratio domains.

This methodology also has significant practical advantages. By eliminating the need for extensive crack propagation calculations and allowing adaptive adjustments to load levels based on direct observation of propagation initiation, test time and postprocessing effort are greatly reduced compared to the ASTM standard. The application of stabilization cycles (N*) before each load increment ensures that the material is conditioned for the new stage, making the previous behavior independent of the test history. The accuracy of the method is contingent upon the number of steps executed within the process. Therefore, to improve accuracy, it is imperative to increase the number of procedural steps undertaken.

6 | Conclusion

In summary, the methodology proposed represents an innovative and more robust alternative to the ASTM E647 standard for the determination of fatigue thresholds. Its focus on the determination of both threshold parameters, $K_{max,th}$ or ΔK_{th}, together with the introduction of the unifying parameter K*, provides a deeper and more accurate understanding of material behavior near the fatigue threshold. The efficiency and reduction in testing and postprocessing requirements make it a promising tool for engineering and structural design applications, although there is a recognized need to extend its validation to a wider range of materials. The fundamental nature of the method, which is based directly on the observation of crack propagation only when both thresholds are satisfied simultaneously, gives it a conceptual robustness that overcomes some of the limitations inherent in the traditional load-on approach. Future research should prioritize the extension of this methodology to a broader range of materials in order to evaluate its applicability, including medium-entropy alloys and brittle metals.

Nomenclature

ΔK	stress intensity factor range
ΔK^+	positive part of the range of the applied SIF
ΔK_{eff}	effective stress intensity factor range
$\Delta K_{eff,th}$	effective threshold stress intensity factor range
ΔK_n	stress intensity factor range at the knee transition point
ΔK_{th}	stress intensity factor range at threshold
CT	compact tension specimen
d_g	grain-size diameter
DTD	damage tolerance design
FCG	fatigue crack growth
K_{cl}	closure stress intensity factor
K_{max}	maximum stress intensity factor
$K_{max,th}$	threshold at maximum stress intensity factor
K_{min}	minimum stress intensity factor
K_{op}	opening stress intensity factor
LEFM	linear-elastic fracture mechanics
OICC	oxide-induced crack closure
PICC	plasticity-induced crack closure
r_c	radius of the cyclic plastic zone
R	load ratio
R_c	critical load ratio
RICC	roughness-induced crack closure
SIF	stress intensity factor

Author Contributions

Conceptualization: P.M.C., A.S.C., and P.L.-C. Methodology: P.M.C. and J.A.A. Data acquisition/curation: P.L.-C. and J.A.A. Formal analysis: P.M.C. and P.L.-C. Writing and editing: P.M.C., J.A.A., A.S.C., and P.L.-C. Resources: P.L.-C. Supervision: A.S.C. and P.L.-C. Project administration: A.S.C. and P.L.-C. Funding acquisition: P.L.-C. Approval: P.M.C., J.A.A., A.S.C., and P.L.-C.

Acknowledgments

Authors would like to acknowledge the following financial support: "FEDER Programa Operativo" by "Junta de Andalucía" (Spain)—grant reference UMA18-FEDERJA-250. Funding for open access charge: Universidad de Malaga/CBUA. This research was also supported by an FPU grant (Formación de Profesorado Universitario) from the Spanish Ministry of Science and Innovation (MCINN) to P.M.C. through grant number FPU23-03834. The authors would also like to acknowledge helpful discussions with Prof. D. Kujawski.

Data Availability Statement

The data that support the findings of this study are available from the corresponding author upon reasonable request.

References

1. ASTM E647-24: *Test Method for Measurement of Fatigue Crack Growth Rates*. 2024.

2. T. L. Anderson and T. L. Anderson, *Fracture Mechanics* (CRC Press, 2005).

3. J. Newman, Jr., J. Schneider, A. Daniel, and D. Mcknight, "Compression Pre-Cracking to Generate Near Threshold Fatigue-Crack-Growth Rates in Two Aluminum Alloys," *International Journal of Fatigue* 27 (2005): 1432–1440.

4. J. C. Newman, Jr., J. J. Ruschau, and M. R. Hill, "Improved Test Method for Very Low Fatigue-Crack-Growth-Rate Data," *Fatigue and Fracture of Engineering Materials and Structures* 34 (2011): 270–279.

5. L. Molent and R. Jones, "The Influence of Cyclic Stress Intensity Threshold on Fatigue Life Scatter," *International Journal of Fatigue* 82 (2016): 748–756.

6. U. Zerbst, M. Vormwald, R. Pippan, H.-P. Gänser, C. Sarrazin-Baudoux, and M. Madia, "About the Fatigue Crack Propagation Threshold of Metals as a Design Criterion—A Review," *Engineering Fracture Mechanics* 153 (2016): 190–243.

7. M. Vormwald, "Elastic-Plastic Fatigue Crack Growth," *Advanced Methods of Fatigue Assessment* (Springer, 2013), 391–481.

8. S. Suresh and R. O. Ritchie, "Propagation of Short Fatigue Cracks," *International Metals Reviews* 29 (1984): 445–475.

9. S. Pearson, "Initiation of Fatigue Cracks in Commercial Aluminium Alloys and the Subsequent Propagation of Very Short Cracks," *Engineering Fracture Mechanics* 7 (1975): 235–247.

10. S. J. Hudak, A. Saxena, R. J. Bucci, and R. C. Malcolm, *Development of Standard Methods of Testing and Analyzing Fatigue Crack Growth Rate Data*. DTIC Document, (DTIC, 1978).

11. D. Taylor, "The Measurement of Near-Threshold Fatigue Crack Growth," *Engineering Fracture Mechanics* 32 (1989): 177–181.

12. D. L., Davidson and S, Suresh. *Fatigue Crack Growth Threshold Concepts*. (Metallurgical Society Inc., 1984).

13. P. K. Liaw, T. R. Leax, R. S. Williams, and M. G. Peck, "Near-Threshold Fatigue Crack Growth Behavior in Copper," *Metallurgical Transactions A* 13 (1982): 1607–1618.

14. D. Kujawski, "A New (ΔK+Kmax)0.5 Driving Force Parameter for Crack Growth in Aluminum Alloys," *International Journal of Fatigue* 23 (2001): 733–740.

15. R. A. Schmidt and P. C. Paris, "Threshold for Fatigue Crack Propagation and the Effects of Load Ratio and Frequency," in *Progress in Flaw Growth and Fracture Toughness Testing* (ASTM International 100 Barr Harbor Drive, PO Box C700, 1973), 79–94.

16. A. K. Vasudévan and S. Suresh, "Influence of Corrosion Deposits on Near-Threshold Fatigue Crack Growth Behavior in 2xxx and 7xxx Series Aluminum Alloys," *Metallurgical Transactions A* 13 (1982): 2271–2280.

17. International Organization for Standardization, *Metallic Materials: Fatigue Testing: Fatigue Crack Growth Method*. ISO 12108 (ISO, 2022).

18. T. Christman and S. Suresh, "Crack Initiation Under Far-Field Cyclic Compression and the Study of Short Fatigue Cracks," *Engineering Fracture Mechanics* 23 (1986): 953–964.

19. S. Suresh, "Crack Initiation in Cyclic Compression and Its Applications," *Engineering Fracture Mechanics* 21 (1985): 453–463.

20. S. (S.) Suresh, *Fatigue of Materials* (Cambridge University Press, 1998).

21. W. A. Herman, R. W. Hertzberg, and R. Jaccard, "A Simplified Laboratory Approach for the Prediction of Short Crack Behavior in Engineering Structures," *Fatigue and Fracture of Engineering Materials and Structures* 11 (1988): 303–320.

22. R. Pippan, F. O. Riemelmoser, and C. Bichler, "Measurability of Crack Closure," *ASTM Special Technical Publication* 1343 (1999): 41–56.

23. J. Newman, "Analyses of Fatigue Crack Growth and Closure Near Threshold Conditions for Large-Crack Behavior," in *Fatigue Crack Growth Thresholds, Endurance Limits, and Design* (ASTM International100 Barr Harbor Drive, PO Box C700, 2000), 227–251.

24. R. J. Asaro, L. Hermann, and J. M. Baik, "Transitions in Fatigue Crack Closure in 2048 Aluminum," *Metallurgical Transactions A* 12 (1981): 1133–1135.

25. S. Suresh, A. K. Vasudévan, and P. E. Bretz, "Mechanisms of Slow Fatigue Crack Growth in High Strength Aluminum Alloys: Role of Microstructure and Environment," *Metallurgical Transactions A* 15 (1984): 369–379.

26. R. D. Carter, E. W. Lee, E. A. Starke, and C. J. Beevers, "The Effect of Microstructure and Environment on Fatigue Crack Closure of 7475 Aluminum Alloy," *Metallurgical Transactions A* 15 (1984): 555–563.

27. G. T. Gray, J. C. Williams, and A. W. Thompson, "Roughness-Induced Crack Closure: An Explanation for Microstructurally Sensitive Fatigue Crack Growth," *Metallurgical Transactions A* 14 (1983): 421–433.

28. S. Taira, K. Tanaka, and M. Hoshina, "Grain Size Effect on Crack Nucleation and Growth in Long-Life Fatigue of Low-Carbon Steel," in *Fatigue Mechanisms* (ASTM International, 1979), 135–139.

29. J. Lindigkeit, G. Terlinde, A. Gysler, and G. Lütjering, "The Effect of Grain Size on the Fatigue Crack Propagation Behavior of Age-Hardened Alloys in Inert and Corrosive Environment," *Acta Metallurgica* 27 (1979): 1717–1726.

30. G. R. Yoder, L. A. Cooley, and T. W. Crooker, "Quantitative Analysis of Microstructural Effects on Fatigue Crack Growth in Widmanstätten Ti-6A1-4V and Ti-8Al-1Mo-1V," *Engineering Fracture Mechanics* 11 (1979): 805–816.

31. J. E. King, "Surface Damage and Near-Threshold Fatigue Crack Growth in a Ni-Base Superalloy in Vacuum," *Fatigue and Fracture of Engineering Materials and Structures* 5 (1982): 177–188.

32. A. Khadimallah, J. Petit, N. Hfaiedh, and A. Znaidi, "Characterization of Fatigue Behavior of AA2024-T351 Aluminum Alloy," *Fatigue and Fracture of Engineering Materials and Structures* 46 (2023): 3729–3744.

33. C. A. Rodopoulos, A. T. Kermanidis, E. Statnikov, V. Vityazev, and O. Korolkov, "The Effect of Surface Engineering Treatments on the Fatigue Behavior of 2024-T351 Aluminum Alloy," *Journal of Materials Engineering and Performance* 16 (2007): 30–34.

34. P. R. Paresi, Y. Lou, A. Narayanan, and J. W. Yoon, "Enhanced Constitutive Model for Aeronautic Aluminium Alloy (AA2024-T351) Under High Strain Rates and Elevated Temperatures," *International Journal of Automotive Technology* 20 (2019): 79–87.

35. R. Pippan, "Threshold and Effective Threshold of Fatigue Crack Propagation in ARMCO Iron I: The Influence of Grain Size and Cold Working," *Materials Science and Engineering A* 138 (1991): 1–13.

36. S. Suresh, G. F. Zamiski, and D. R. O. Ritchie, "Oxide-Induced Crack Closure: An Explanation for Near-Threshold Corrosion Fatigue Crack Growth Behavior," *Metallurgical Transactions A* 12 (1981): 1435–1443.

37. R. Pippan and A. Hohenwarter, "Fatigue Crack Closure: A Review of the Physical Phenomena," *Fatigue and Fracture of Engineering Materials and Structures* 40 (2017): 471–495.

38. B. Li and L. G. Rosa, "Prediction Models of Intrinsic Fatigue Threshold in Metal Alloys Examined by Experimental Data," *International Journal of Fatigue* 82 (2016): 616–623.

39. P. B. Chowdhury, H. Sehitoglu, and R. G. Rateick, "Predicting Fatigue Resistance of Nano-Twinned Materials: Part II—Effective Threshold Stress Intensity Factor Range," *International Journal of Fatigue* 68 (2014): 292–301.

40. A. K. Vasudevan, K. Sadananda, and N. Louat, "A Review of Crack Closure, Fatigue Crack Threshold and Related Phenomena," *International Journal of Fatigue* 1 (1996): 62.

41. K. Sadananda, S. Sarkar, D. Kujawski, and A. K. Vasudevan, "A Two-Parameter Analysis of S–N Fatigue Life Using $\Delta\sigma$ and σmax," *International Journal of Fatigue* 31 (2009): 1648–1659.

42. D. Kujawski and A. K. Vasudevan, "A Procedure for Determination of Thresholds: ΔKth and Kmax,th," *International Journal of Fatigue* 142 (2021): 105911.

43. B. Moreno, J. Zapatero, and J. Domínguez, "An Experimental Analysis of Fatigue Crack Growth Under Random Loading," *International Journal of Fatigue* 25 (2003): 597–608.

44. M. Mokhtarishirazabad, P. Lopez-Crespo, and M. Zanganeh, "Stress Intensity Factor Monitoring Under Cyclic Loading by Digital Image Correlation," *Fatigue and Fracture of Engineering Materials and Structures* 41 (2018): 2162–2171.

45. ASTM E399-22: *Test Method for Linear-Elastic Plane-Strain Fracture Toughness of Metallic Materials*. 2022.

46. S. Lubich, C. Fischer, S. Schilli, and T. Seifert, "Microstructure-Sensitive Finite-Element Analysis of Crack-Tip Opening Displacement and Crack Closure for Microstructural Short Fatigue Cracks," *International Journal of Fatigue* 162 (2022): 106911.

47. Y. Hu, H. Cheng, J. Yu, and Z. Yao, "An Experimental Study on Crack Closure Induced by Laser Peening in Pre-Cracked Aluminum Alloy 2024-T351 and Fatigue Life Extension," *International Journal of Fatigue* 130 (2020): 105232.

48. B. Moreno, A. Martin, P. Lopez-Crespo, J. Zapatero, and J. Dominguez, "Estimations of Fatigue Life and Variability Under Random Loading in Aluminum Al-2024T351 Using Strip Yield Models From NASGRO," *International Journal of Fatigue* 91 (2016): 414–422.

49. P. Lopez-Crespo, A. Shterenlikht, J. R. Yates, E. A. Patterson, and P. J. Withers, "Some Experimental Observations on Crack Closure and Crack-Tip Plasticity," *Fatigue and Fracture of Engineering Materials and Structures* 32 (2009): 418–429.

50. M. F. Borges, P. Lopez-Crespo, F. V. Antunes, et al., "Fatigue Crack Propagation Analysis in 2024-T351 Aluminium Alloy Using Nonlinear Parameters," *International Journal of Fatigue* 153 (2021): 106478.

51. D. Kujawski, "A Fatigue Crack Driving Force Parameter With Load Ratio Effects," *International Journal of Fatigue* 23 (2001): 239–246.

52. A. S. Chernyatin, P. Lopez-Crespo, B. Moreno, and Y. G. Matvienko, "Multi-Approach Study of Crack-Tip Mechanics on Aluminium 2024 Alloy," *Theoretical and Applied Fracture Mechanics* 98 (2018): 38–47.

53. T. C. Lindley and C. E. Richards, "The Relevance of Crack Closure to Fatigue Crack Propagation," *Materials Science and Engineering* 14 (1974): 281–293.

54. A. J. McEvily, "Current Aspects of Fatigue," *Metal Science* 11 (1977): 274–284.

55. B. L. Boyce and R. O. Ritchie, "Effect of Load Ratio and Maximum Stress Intensity on the Fatigue Threshold in Ti–6Al–4V," *Engineering Fracture Mechanics* 68 (2001): 129–147.

56. R. Pippan and A. Hohenwarter, "Modeling of Fatigue Crack Growth: Dislocation Models," in *Comprehensive Structural Integrity* (Elsevier, 2023), 56–70.

57. R. W. Hertzberg, "On the Calculation of Closure-Free Fatigue Crack Propagation Data in Monolithic Metal Alloys," *Materials Science and Engineering A* 190 (1995): 25–32.

58. M.-L. Zhu, F.-Z. Xuan, and S.-T. Tu, "Effect of Load Ratio on Fatigue Crack Growth in the Near-Threshold Regime: A Literature Review, and a Combined Crack Closure and Driving Force Approach," *Engineering Fracture Mechanics* 141 (2015): 57–77.

59. L. Lawson, "Near-Threshold Fatigue: A Review," *International Journal of Fatigue* 21 (1999): 15–34.